TOWARDS NUMERICAL SIMULATION OF CAVITATING FLOWS IN COMPLEX GEOMETRIES

Aswin Gnanaskandan
Dept. of Aerospace Engineering and Mechanics
University of Minnesota
Minneapolis, Minnesota-55455
Email:gnan0009@aem.umn.edu.

Krishnan Mahesh
Dept. of Aerospace Engineering and Mechanics
University of Minnesota
Minneapolis, Minnesota-55455
Email:mahesh@aem.umn.edu

SUMMARY

We are developing the DNS/LES capability for turbulent cavitating flows in complex geometries. The multiphase medium is represented using a homogeneous equilibrium model that assumes thermal equilibrium between the liquid and the vapor phase. The governing equations are the compressible Navier Stokes equations for the liquid/vapor mixture along with a transport equation for the vapor mass fraction. A separate energy equation is solved, as opposed to assuming isothermal flow. The unstructured compressible algorithm in [1] has been extended to solve for multiphase flows. A characteristic filter based shock capturing scheme is developed to handle shocks and contact discontinuities in non-ideal gases and mixtures. The shock capturing is applied in a predictor-corrector approach, where the base scheme is non-dissipative and symmetric. The numerical method is validated for benchmark problems and applied to a cavitating flow over a circular cylinder.

INTRODUCTION

Cavitation occurs in a wide variety of situations. e.g. inside vortices, in valves, behind orifices and on propulsor blades. The physical consequences include noise, vibration and surface erosion. One approach to physically model cavitating flows is the homogeneous mixture model [2, 3] where the mixture of water and vapor is modeled as a compressible fluid. High fidelity turbulent cavitating flow simulations are very challenging. Turbulence has a broadband spectrum which requires non dissipative numerical schemes to represent smaller scales accurately. However non dissipative schemes become unstable at high Reynolds numbers. Furthermore, cavitation is characterized by large gradients in density, and strong shock waves that form during vapor cloud collapse. These challenges are compounded by complex geometries. An algorithm that addresses these challenges is developed. Complex geometries are represented by unstructured grids. A novel predictor corrector characteristic filter based shock capturing scheme is developed for the mixture of vapor and water to handle contact discontinuities and shock waves. The

predictor step is non dissipative and discretely energy conserving which makes it both robust and accurate at high Reynolds numbers. Also, the total energy equation is solved instead of invoking the isothermal assumption, as is commonly done.

This paper discusses our numerical method, validates it for benchmark problems and applies it to study cavitation behind a circular cylinder. The paper is organized as follows. The 'Numerical method' section outlines the governing equations along with the source terms for evaporation of water and condensation of vapor. It also discusses the characteristic filter based shock capturing method applied to multiphase flows. The 'Results and Discussion' section discusses the numerical validation of the method using a multicomponent shock tube problem and a multiphase shock tube problem. Finally the algorithm is applied to study cavitation behind a circular cylinder for three different cavitation numbers.

NUMERICAL METHOD
Governing Equations

The governing equations are the compressible Navier Stokes equations along with an advection equation for mass fraction of vapor.

$$\frac{\partial \rho}{\partial t} = -\frac{\partial}{\partial x_k}(\rho u_k)$$
$$\frac{\partial \rho u_i}{\partial t} = -\frac{\partial}{\partial x_k}(\rho u_i u_k + p\delta_{ik} - \sigma_{ik})$$
$$\frac{\partial E_T}{\partial t} = -\frac{\partial}{\partial x_k}\{(E_T + p)u_k - \sigma_{ik}u_i - Q_k\} \quad (1)$$
$$\frac{\partial \rho Y}{\partial t} = -\frac{\partial}{\partial x_k}(\rho Y u_k) + S_e - S_c$$

where ρ, u_i, p, E_T and Y are density, velocity, pressure, total energy and mass fraction of vapor, respectively. The viscous stress

σ_{ij} and heat flux Q_i are given by

$$\sigma_{ij} = \mu\left(\frac{\partial u_i}{\partial x_j} + \frac{\partial u_j}{\partial x_i} - \frac{2}{3}\frac{\partial u_k}{\partial x_k}\delta_{ij}\right), \tag{2}$$

$$Q_i = k\frac{\partial T}{\partial x_i}. \tag{3}$$

S_e and S_c are source terms for evaporation of water and condensation of vapor given by

$$S_e = 0.1\alpha^2(1-\alpha)^2\frac{\rho_l}{\rho_g}\frac{\max((p_v - p),0)}{\sqrt{2\pi R_g T}} \tag{4}$$

$$S_c = 0.1\alpha^2(1-\alpha)^2\frac{\max((p_v - p),0)}{\sqrt{2\pi R_g T}} \tag{5}$$

where α is the volume fraction of vapor and p_v is the vapor pressure given by

$$p_v = p_k\exp((1-\frac{T_k}{T})(a+(b-cT)(T-d)^2)) \tag{6}$$

where p_k = 22.130 Mpa , T_k = 647.31 K , a = 7.21, b = 1.152e-5, c = -4.787e-9, d = 483.16. The equation of state for the mixture of vapor and water is given by the summation of partial pressure of the individual phases:

$$p = Y\rho R_g T + (1-Y)\rho K_l T\frac{p}{p+P_c} \tag{7}$$

where R_g, K_l and P_c are constants associated with the equation of state of vapor and liquid.

The relation for speed of sound in the mixture is obtained from the equation of state using the Gibbs equation and is given by

$$a^2 = \frac{C_1 T}{C_0 - \dfrac{C_1}{C_{pm}}}, \text{where}$$

$$C_0 = 1 - (1-Y)\rho K_l T\frac{P_c}{(p+P_c)^2} \tag{8}$$

$$C_1 = R_g Y - K_l(1-Y)\frac{P}{p+P_c}$$

$$C_{pm} = YC_{pg} + (1-Y)C_{pl}.$$

The dimensionless form of the governing equations are discretized using a cell-centered finite volume scheme. The simulations employ a modified least-square method for face reconstruction, which is more accurate than a simple symmetric reconstruction, and more stable than a least square reconstruction. The solution is advanced in time using a second-order explicit Adams-Bashforth scheme.

Characteristic Filter based Shock Capturing

The predictor step described above is non-dissipative and hence cannot capture discontinuities. An external shock capturing mechanism is therefore provided. The characteristic filter based shock capturing [4] was extended to unstructured grids for ideal gases in [1]. This method has further been extended to non-ideal gases and mixtures of fluids. A non linear filter has been implemented independent of the base scheme in a predictor corrector method. The main advantage of using a non linear filter over a linear filter is that the amount of dissipation applied to each equation is controlled separately based on the characteristics and hence there is a better control over the numerical dissipation. The dissipation is further localized to regions of large divergence and large gradients of mass fraction. Once a physical time step Δt is advanced to get the solution $\widehat{q}^{n+1}$ from q^n, the final solution q^{n+1} at $t + \Delta t$ is obtained from a corrector step

$$q_{cv}^{n+1} = \widehat{q}_{cv}^{n+1} - \frac{\Delta t}{V_{cv}}\sum_{\text{faces}}(F_f^*.n_f)A_f \tag{9}$$

where F_f^* is the filtered numerical flux of the following form

$$F_{fc}^* = \frac{1}{2}R_{fc}\Phi_{fc}^*. \tag{10}$$

Here, R_{fc} is the right eigenvector vector at the face computed using Roe-average of left and right control volumes. The expression for the l th component of Φ^*, ϕ^{*l} is given by

$$\phi_{fc}^{*l} = k\theta_{fc}^l\phi_{fc}^l \tag{11}$$

where, k is an adjustable parameter and θ_{fc} is the switch function given by

$$\theta_{fc} = \sqrt{0.5(\widehat{\theta}_{icv1}^2 + \widehat{\theta}_{icv2}^2)}$$

$$\widehat{\theta}_{icv1} = \frac{|\alpha_{fc}| - |\alpha_{f1}|}{|\alpha_{fc}| + |\alpha_{f1}|} \tag{12}$$

$$\widehat{\theta}_{icv2} = \frac{|\alpha_{f2}| - |\alpha_{fc}|}{|\alpha_{f2}| + |\alpha_{fc}|}.$$

Here, $\alpha_f = R_f^{-1}(q_{icv2} - q_{icv1})$ is the difference between characteristic variables across the face. The subscript 'fc' stands for the face for which fluxes are being calculated and subscripts 'f1' and 'f2' stand for the two most parallel faces to the face 'fc'. Further details on implementation of the characteristic filter based shock capturing may be found in [1].

RESULTS & DISCUSSION
Numerical Validation

Speed of Sound : The speed of sound obtained from the equation of state is compared with the experimental data in [5] and is presented in Figure 1. It can be observed that the speed of
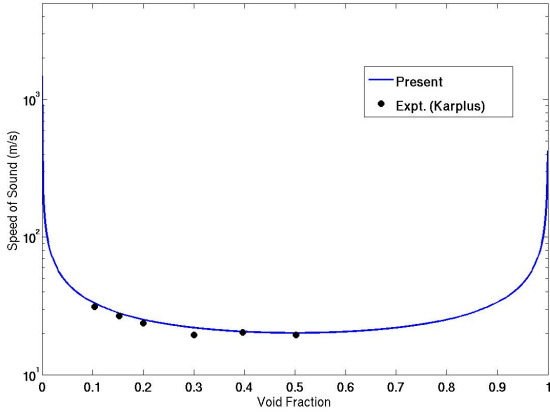
2

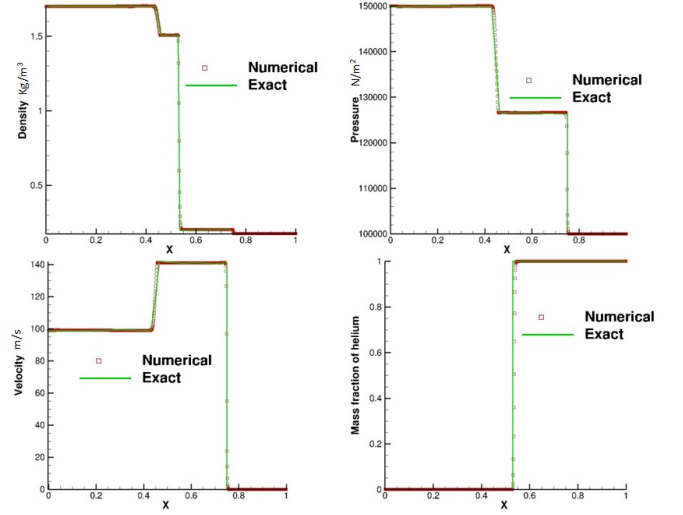**Figure 1**. Speed of sound in water and vapor mixture.

Figure 2. Results for air-helium shock tube.

Figure 3. Results for air-water shock tube.

sound in water is close to 1500 m/s and that in vapor is about 486 m/s. On addition of even a small amount of vapor, the speed of sound in the mixture reduces to about 30 m/s and this low speed of sound can yield locally supersonic regions in cavitating flows.

Multicomponent Shock tube : A one dimensional shock tube [6] with air on one side of the interface and helium on the other side is simulated. The shock wave refracts at the gas interface, leading to a transmitted and a reflected shock wave. The transmitted shock wave will travel faster or slower than the incident shock wave depending on the speed of sound in the fluids. The initial conditions correspond to a weak shock wave with a Mach number $M_s = 1.1952$ in air propagating towards a region occupied by helium. The computational domain is discretized uniformly using 1000 cells. The initial conditions are given by

$$Q = [\rho, u, P, \gamma, Y]$$
$$Q_{A1} = [1.7017, 98.956, 1.5.10^5, 1.4, 0.0]$$
$$Q_{A2} = [1.2763, 0.000, 1.0.10^5, 1.4, 0.0] \quad (13)$$
$$Q_{He} = [0.1760, 0.000, 1.0.10^5, 1.67, 0.0].$$

Figure 2 shows the comparison of numerical and exact solution at t = 864μs. The comparison shows that the numerical method is able to accurately capture shock waves and contact discontinuities. The transmitted shock wave travels faster than the incident shock wave since the acoustic speed in helium is greater than that in air.

Multiphase shock tube : A two phase shock tube [7] with water and compressed air is simulated. The driver section contains liquid water at high pressure and the driven section contains compressed air at lower pressure. The density and pressure differ by ratio a of 20 and 10^4 across the discontinuities. The computational domain is discretized uniformly using 1000 cells and the
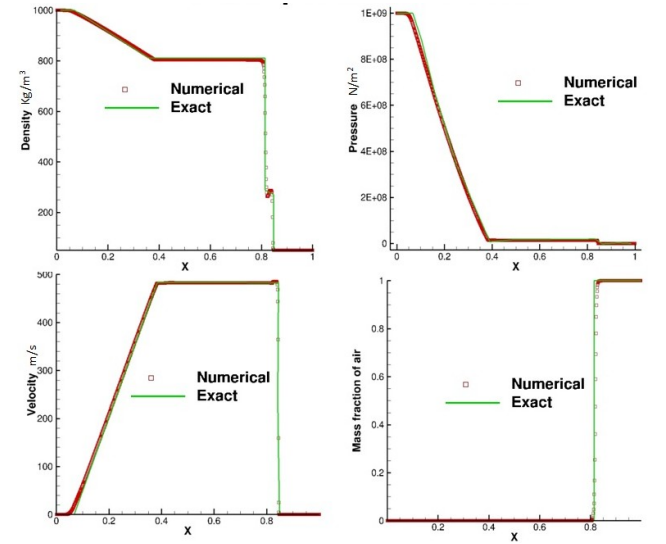
initial conditions are given by

$$Q = [\rho, u, P, \gamma, Y]$$
$$Q_W = [1000, 0, 1.5.10^9, 4.4, 0.0] \quad (14)$$
$$Q_A = [50, 0, 1.0.10^5, 1.4, 1.0].$$

Figure 3 shows the comparison between numerical and exact solution at 240 μs. Although the jumps agree very well with the analytical results, small oscillations in density, velocity and pressure are seen near the contact discontinuity. This is a characteristic feature of conservative schemes applied to multi component flows. It occurs due to the fact that two different equations of state are used on either side of the contact discontinuity. The average pressure calculated from these left and right values will obviously not be the actual average pressure and this leads to an oscillation in pressure. A remedy to overcome this issue is given in [7].
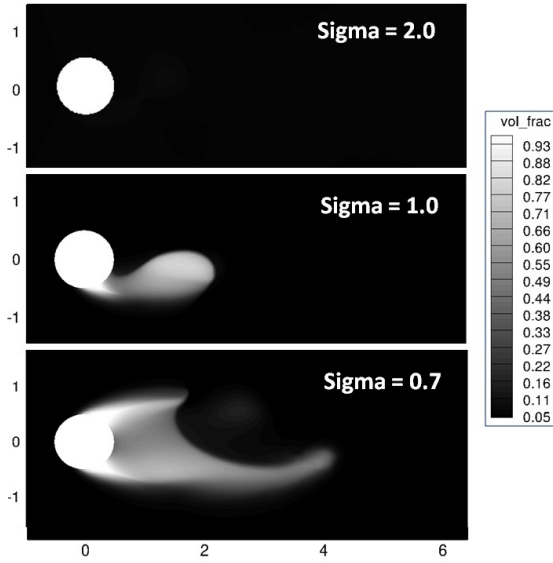
3

Figure 4. Instantaneous void fraction contours.

Figure 5. Pressure and void fraction variation across a contact discontinuity.

Cavitating Flow over a Circular Cylinder

A cavitating flow past a 2D circular cylinder is simulated. An ambient void fraction of $\alpha_0 = 0.01$ and ambient temperature of 300 K is assumed. The Reynolds number of the flow is ($Re_D = \frac{\rho_0 U_0 D}{\mu_0}$) 200, where D is the diameter of the cylinder. Numerical simulations have been performed for three cases pertaining to cavitation numbers ($\sigma = \frac{p_\infty - p_v}{0.5\rho_0 u_0^2}$) of 2.0, 1.0 and 0.7 corresponding to the simulations carried out in [8]. The cavitation numbers are varied by varying the inlet velocity keeping all other quantities constant. The domain is discretized using a C-grid. The near wall spacing in the radial and circumferential directions are 0.01 D. The length of the domain is 20 D in the upstream, top and bottom and 30 D in the downstream directions in order to capture the wake behind the cylinder. Free stream boundary conditions are applied at the inlet and zero gradient conditions are applied in the outlet, top and bottom boundaries. Non-reflecting sponge boundary conditions are applied at all the free stream boundaries to prevent any reflection of acoustic waves from the boundary into the domain.

Figure 4 shows the instantaneous void fraction contours for all three cases. $\sigma = 2.0$ corresponds to a non cavitating case since the pressure never falls below vapor pressure and hence there is no vapor, while $\sigma = 1.0$ and 0.7 correspond to cavitating cases. Although the mean pressure for $\sigma = 1.0$ does not fall below vapor pressure, the unsteady pressure falls below vapor pressure and hence a vapor cavity is formed periodically in the wake of the cylinder. For $\sigma = 0.7$, the mean pressure in the wake is less than the vapor pressure and hence a vapor cavity is present in the wake at all times.

As discussed above, a conservative scheme can cause spurious oscillations in pressure across a contact discontinuity. Hence it is important to verify if the error in pressure across a contact discontinuity is small. Figure 5 shows void fraction and pressure plotted against the horizontal distance on a generator line which cuts through a vapor cloud 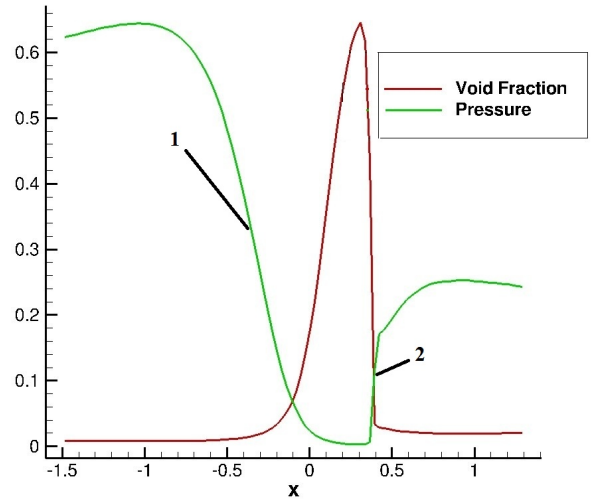in the $\sigma = 1.0$ case. It is very clear that there are two phase channge processes, one from liquid to vapor marked as 1 and the other from vapor to liquid marked as 2. The first phase change from liquid to vapor is cavitation and there is no large pressure change associated with this phenomenon. The second phase change is the condensation of vapor into liquid. This is the cavity collapse that results in a shock which involves a large pressure gradient. Both phase change processes are free of pressure oscillations. Hence the error across a contact discontinuity due to the conservative scheme is small. The temperature rise across the shock is 2% of the free stream temperature.

Figure 6 shows the unsteady characteristics of the flow in the form of lift and drag history for all three cases. Since $\sigma = 2.0$ is non cavitating, the lift and drag profiles are perfect sinusoids as in a single phase flow, the C_L curve yielding the Strouhal number corresponding to vortex shedding $St = 0.19$. The lift and drag profiles of the cavitating cases are significantly affected by cavitation. The profile for $\sigma = 1.0$ still remains periodic in time, but the Strouhal number corresponding to vortex shedding is reduced to 0.16 which agrees well with [8]. The peaks in the middle of a cycle are due to the fact that the shock wave created due to vapor collapse impinges on the surface. For $\sigma = 0.7$, the profiles are no longer periodic because of a low frequency phenomenon occurring at a Strouhal number of approximately 0.03. This low frequency phenomenon is associated with the behaviour of the vapor cavity in the wake [8]. The Strouhal number corresponding to vortex shedding is approximately 0.13.

Figure 7 shows the dynamics of the cavity formation and collapse for $\sigma = 1.0$. This figure shows void fraction contours, pressure contours and the corresponding instant in the load cycle for various instants of time. In the figure, (a) shows the impending collapse of the vapor cavity as it gets thinner in the middle. (b) shows the subsequent collapse of the cavity leading to two separate smaller regions of vapor marked as Cav 1 and Cav 2. This collapse causes a shock wave (Shk 1) that propagates outwards. By this time, the separated cavity (Cav 2) also collapses leading to another shock wave (Shk 2) as shown in (c). (d) shows the fully formed vapor cavity on the top half of the cylinder and this
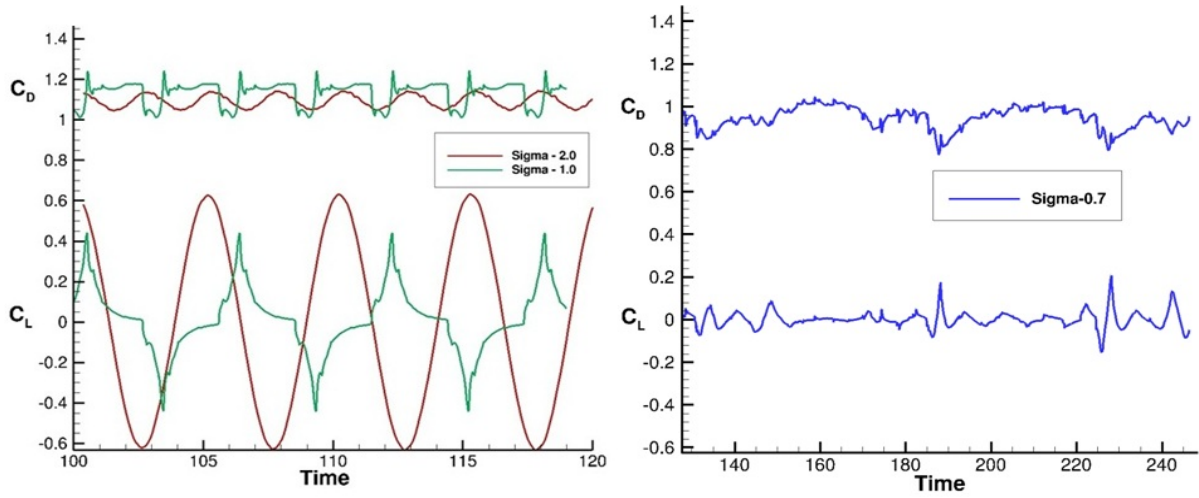
Figure 6. Variation of lift coefficient (C_L) and drag coefficient (C_D) with time.
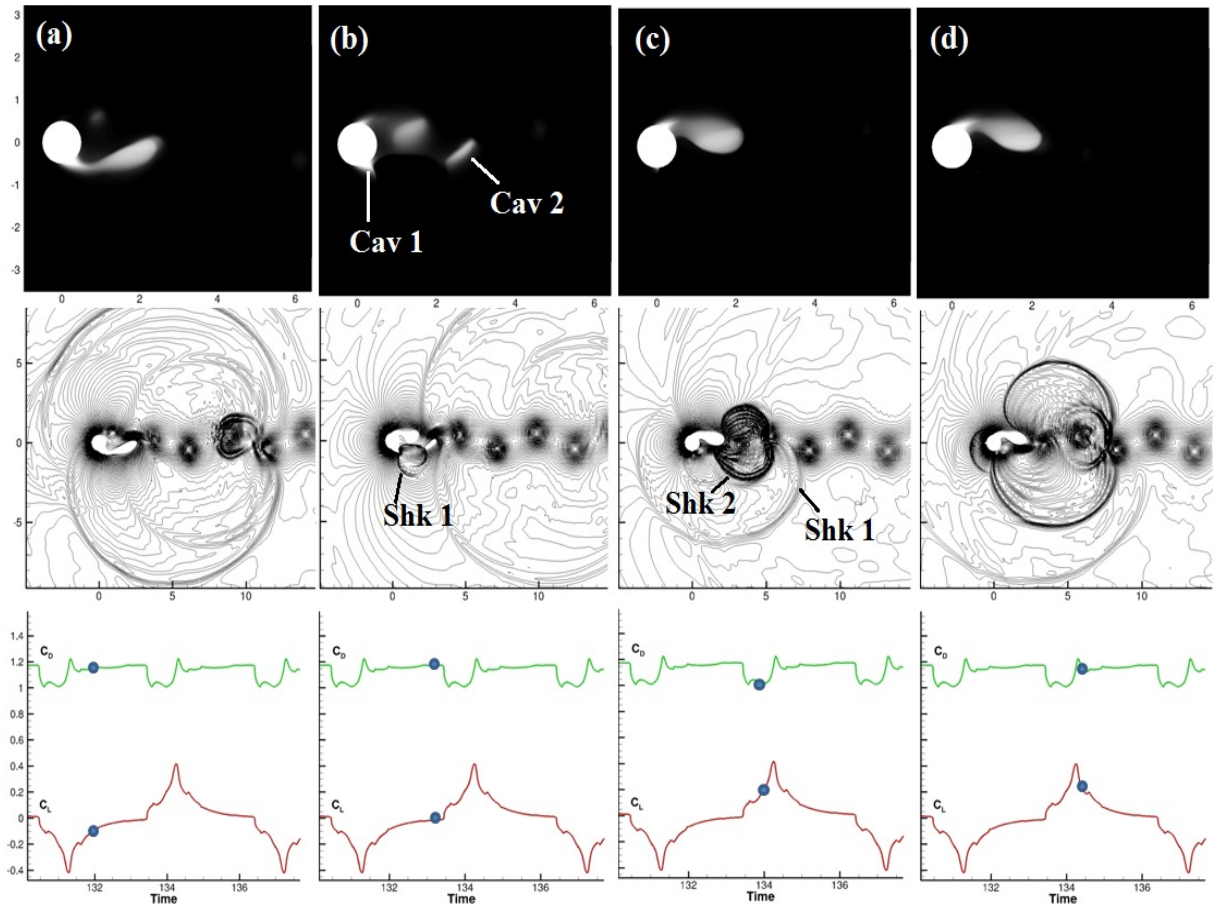

Figure 7. Illustration of vapor cloud collapse and shock formation for $\sigma = 1.0$.

entire cycle repeats itself.

Figure 8 shows the dynamics of the cavity formation and collapse for $\sigma = 0.7$. Void fraction contours, pressure contours and their corresponding instant in the load cycle are shown for various instants of time. In the figure, (a) shows the fully formed cavity and the corresponding pressure contour shows shocks from the

previous cycle propagating outwards. In (b), the cavity (Cav 1) gets elongated and the rear end of Cav 1 collapses in (c) giving rise to a shock (Shk 1). By this time, the vapor region in the bottom half grows and merges with Cav 1 leading to much bigger cavity which fills the entire wake before the entire cycle repeats again.
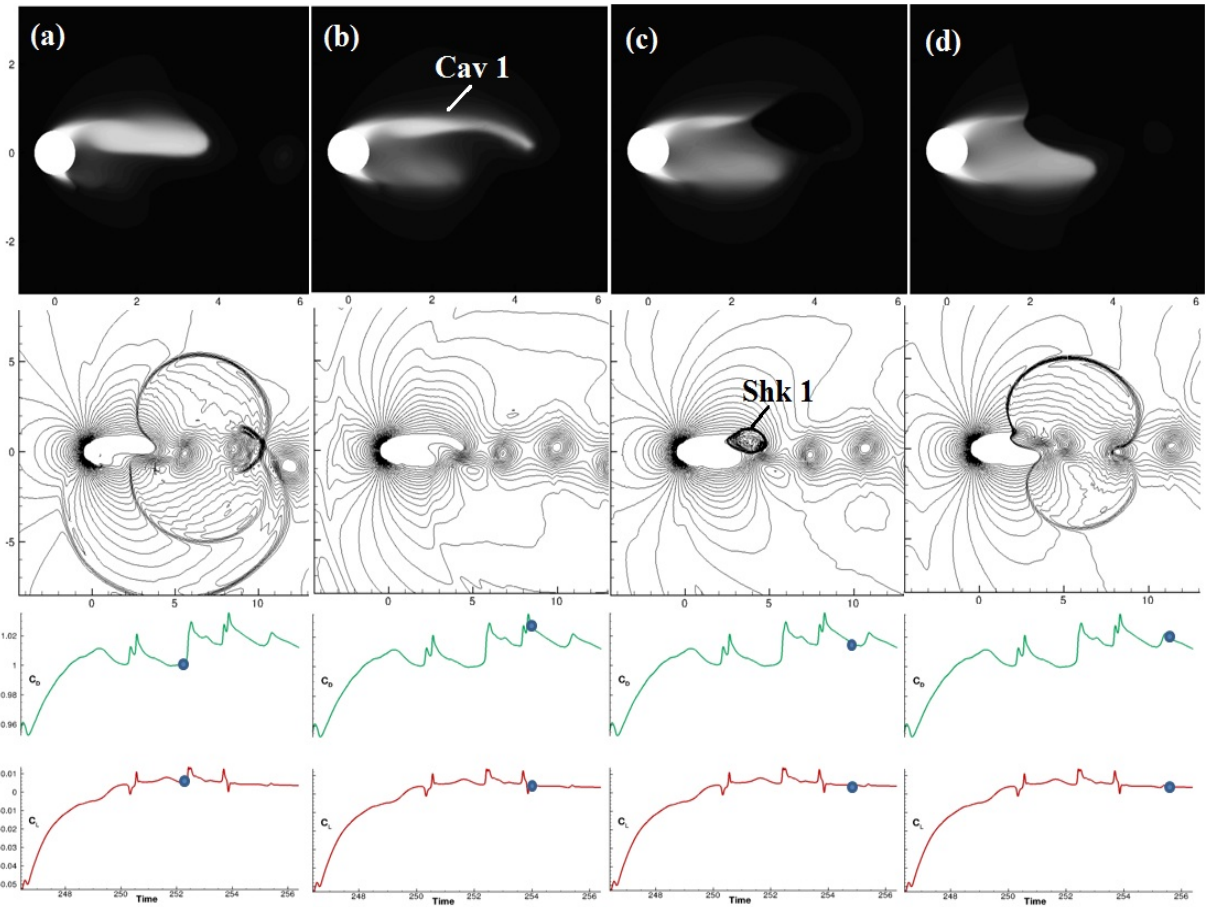
5

Figure 8. Illustration of vapor cloud collapse and shock formation for $\sigma = 0.7$.

CONCLUSIONS

A numerical method has been developed to simulate multicomponent and cavitating flows using homogeneous equilibrium method. The mixture of water and vapor is described as a compressible fluid using a mixture equation of state. A characteristic filter based shock capturing method has been developed for a mixture of fluids and is applied in a predictor corrector method to limit the dissipation to the vicinity of shocks and contact discontinuities. The method has been validated by simulating one dimensional shock tube problems and two dimensional cavitating flow over a circular cylinder. The cavitating flow over a cylinder leads to vapor cavity formation which on subsequent collapse emits shock waves. Cavitation also results in a change in the vortex shedding frequency.

REFERENCES

[1] Park, N. and Mahesh, K., 2007. "Numerical and modeling issues in LES of compressible turbulence on unstructured grids". *AIAA, 2007-722*, Nov.

[2] Saito, Y.,Takami, R.,Kakamori, I. and Ikohagi, T, 2007. "Numerical analysis of unsteady behaviour of cloud cavitation around NACA0015 foil". *J. Comput. Mech, 40, 85-96*.

[3] Seo, J.H. and Lele, S.K, 2009. "Numerical investigation of cloud cavitation and cavitation noise on a hydrofoil section". *Proceedings of the 7th International Symposium on Cavitation*.

[4] Yee, H.C.,Sandham, N.D. and Djomehri, M.J., 1999. "Low-dissipative high-order shock-capturing methods using characteristic-based filters". *J. Comput. Phy, 150, 199-238*.

[5] Karplus, H.B., 1958. "The velocity of sound in liquid containing gas bubbles". *Armour Research Foundation of Illinois, C00-248*.

[6] Lagumbay, R.S.,Vasilyev, O.V. and Haselbacher, A., 2007. "Homogenous equillibrium mixture model for simualtion of multiphase/multicomponent flows". *Int. J. Numer. Meth, 00, 1-6*.

[7] Abgrall, R. and Karni, S., 2001. "Computation of compressible multifluids". *J. Comput. Phy, 169, 594-623*.

[8] Seo, J.H.,Moon, Y.J. and Shin, B.R., 2008. "Prediction of cavitating flow noise by direct numerical simulation". *J. Comput. Phy, 227, 6511-6531*.